Fault-tolerant Control for Non-sinusoidal Multiphase Drives with Minimum Torque Ripple

Duc Tan Vu, *Member*, *IEEE*, Ngac Ky Nguyen, *Member*, *IEEE*, and Eric Semail, *Member*, *IEEE*

***Abstract*- For non-sinusoidal electromotive force (NS-EMF) multiphase machines, this paper proposes a new strategy and control scheme to guarantee smooth torque under an open-phase fault. Notably, the conventional proportional-integral (PI) controllers implemented for vector control in healthy mode can be used in the faulty mode. The strategy is based on reduced-order transformations while the control scheme applies a simple artificial intelligence algorithm using a specific online-trained Adaptive Linear Neuron (ADALINE). Indeed, the inputs of ADALINE require the knowledge of rotor position and NS-EMF harmonic rank to optimize the learning time. The proposed strategy and control scheme are tested on a seven-phase machine with a strong Total Harmonic Distortion (THD) of NS-EMFs, containing numerous harmonics H*k* (THD=38% with 100% H1, 32.3% H3, 9.4% H7, 12.5% H9, 10.3% H11). Numerical and experimental results are presented in this paper. This paper is accompanied by a video demonstrating the experimental results.**

***Index Terms*-Multiphase machine, seven-phase machine, non-sinusoidal electromotive force, fault-tolerant control, reduced-order transformation, adaptive linear neuron.**

I. Introduction

The use of sinusoidal electromotive forces (S-EMFs) impacts the cost of the machine because S-EMFs not only induce constraints on machine design and manufacturing but also lead to a non-optimal use of magnets. For emerging electrical automotive mass-market, machines with non-sinusoidal electromotive forces (NS-EMFs) are attractive but pulsating torques appear. Therefore, S-EMF three-phase machines are usually chosen with vector control, using proportional-integral (PI) controllers in rotating (d-q) frames. With a *n*-phase machine, high-quality vector control can be generalized in multi-rotating frames even with NS-EMFs. More precisely, NS-EMFs containing maximum $(n+1)/2$ (n is odd) and $(n+2)/2$ (n is even) harmonics can be accepted [1]. Therefore, the constraints on the EMF harmonic spectrum are alleviated when n increases. Moreover, as fault tolerance is provided with a multiphase machine, safety margins on power components can be reduced since a failure does not lead to a drive breakdown. Nevertheless, in faulty mode, the requirement for smooth torque is more difficult to be satisfied with NS-EMFs. Consequently, a reconfiguration with new reference currents is required to ensure smooth torque, but these currents are usually complex and time-variant in rotating frames. The strategies to find new reference currents for open circuit faults can be generally classified into three strategy groups based on Fig. 1. After examining different existing strategies, we will propose an approach dedicated to NS-EMFs.

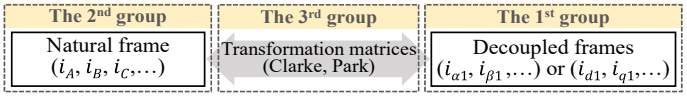

Fig. 1. Three fault-tolerant strategy groups based on transformations of currents between natural and decoupled frames.

The first strategy group is to determine new reference currents in decoupled frames using classical transformation matrices. Remaining healthy phase currents have unidentical waveforms. Main sinusoidal magnetomotive forces (MMFs) generating most of the torque are preserved. In other words, main reference d-q currents are time-constant to facilitate current control. However, other d-q currents are forcedly time-variant, potentially causing torque ripples. This approach was early presented in [2, 3] for induction machines, and has been more recently described in [4-6] for permanent magnet synchronous machines (PMSMs). For example, in [4], four main constant d-q currents are preserved for torque generation in a post-fault 7-phase machine. However, other two d-q currents must be time-variant. If NS-EMF harmonics associated with the two varying currents are significant, torque ripples are inevitably generated as described in [5] (>30%). Therefore, varying reference d-q currents in the first strategy group not only pose challenges for PI controllers but also generate torque ripples with multi-harmonics in NS-EMFs.

The second group of fault-tolerant strategies is to define new reference currents in natural frame while the classical transformation matrices are preserved. Remaining healthy phase currents can be directly defined either to obtain a constant torque or to have an expected current waveform. The approach with a constant torque [7-11], regardless of multi-harmonics in NS-EMFs, results in arbitrary current waveforms like the first group strategies. Meanwhile, if an expected current waveform is considered, current amplitudes and copper losses can be imposed as in [5] but the torque is possibly no longer constant with NS-EMFs. Especially, different from the first group, all reference d-q currents in the second group are time-variant [5, 7-11], making current control design with PI controllers difficult at different operating points.

Duc Tan Vu, Ngac Ky Nguyen, and Eric Semail are with Laboratory of Electrical Engineering and Power Electronics (L2EP), University of Lille, Arts et Metiers Institute of Technology, Centrale Lille, Yncrea Hauts-de-France, ULR 2697-L2EP, HESAM, F-59000 Lille, France (email: duc_tan.vu@ensam.eu; ngacky.nguyen@ensam.eu; eric.semail@ensam.eu). Duc Tan Vu is also with Thai Nguyen University of Technology, Thai Nguyen University, Thai Nguyen, Vietnam (email: vuductan-tdh@tnut.edu.vn).

This work has been achieved within the framework of CE2I project. CE2I is co-financed by European Union with the financial support of European Regional Development Fund (ERDF), French State and the French Region of Hauts-de-France.

In the third strategy group, new reference currents are determined by finding new transformation matrices. For example, new reference currents for a n-phase machine with one opened phase are determined by finding new (n-1)-by-(n-1) transformation matrices. In other words, a post-fault n-phase machine is considered as an asymmetrical (n-1)-phase machine. The new matrices are defined according to the preservation of sinusoidal MMFs as in healthy mode. The orthogonality between rows of the new matrices must be guaranteed for new decoupled frames. Most studies in this group deal with 5-phase S-EMF machines [12-20] and a constant torque is generated by sinusoidal phase currents. Notably, [20] proposes a general approach to find new transformation matrices to obtain constant reference d-q currents with sinusoidal phase currents. However, for NS-EMFs, high-ripple torques are significantly generated due to interactions between NS-EMF harmonics and the fundamental current as analyzed in [21]. Only a few studies [22-24] consider 5-phase NS-EMF machines with the presence of the third harmonic. New reference currents are calculated to obtain constant torques but all reference d-q currents for control are time-variant. Therefore, the control of varying reference currents is a challenge in the third strategy group.

To sum up, the three above strategy groups, in case of NS-EMFs, deal with varying reference d-q currents that possibly generate torque ripples and pose challenges for control. It is difficult to control varying reference d-q currents with conventional PI controllers when the speed increases, making a high demand for higher bandwidth controllers. If PI controllers are applied as in [22], high-ripple torques are inevitable, especially at high speed. It is possible to completely change the control by using a simple solution with hysteresis controllers as presented in [3, 7, 8, 25]. Nevertheless, hysteresis controllers have inevitable variable switching frequencies, high switching losses, and electromagnetic compatibility problems. Therefore, this solution can be used for low-power applications. Model Predictive Control (MPC) is another solution as presented in [13, 19]. Due to a high number of iterations, MPC possesses high computational costs, especially in case of multiphase drives. It also requires accurate system knowledge for the model prediction, and it has high switching frequencies. Resonant PI (PIR) controllers can track varying currents in faulty conditions for 5-phase machines [13, 23, 24, 26]. However, in general, PIR requires accurate estimations of the frequency and parameter-tuning procedures, and it has a poor performance in dynamic states.

In [27], reference currents for 6-phase machines in faulty modes are tracked by Artificial Intelligence (AI) combined with fuzzy logic control. Despite a good tracking performance, specific knowledge is required for parameter setup, and the calculation burden is a challenge. Meanwhile, adaptive linear neuron (ADALINE), a simple type of AI, can be a suitable solution. ADALINE possesses several outstanding advantages [10, 28-30] such as self-learning, fast convergence, and simple implementation in real-time systems if their inputs are well chosen. ADALINE weights are constant in steady states and fast converge in transient states.

TABLE I
CONSIDERED COMPARATIVE CASES IN THIS STUDY

Case	Description
1	Healthy mode using constant reference d-q currents with MTPA [7, 8] in the conventional RFOC scheme*
2	One phase is open-circuited without any reconfigurations
3	Imposing new varying reference d-q currents with MTPA [7, 8] in the pre-fault control scheme*
4	Imposing new varying reference d-q currents with the proposed RCA in the pre-fault control scheme*
5	Imposing new constant reference d-q currents with the proposed RCA in the proposed ADALINE-based control scheme

*The pre-fault control scheme is the RFOC scheme used in healthy mode.

In this paper, the idea is to preserve the conventional PI controllers using constant reference currents in faulty mode with minimum torque ripple. A reconfiguration strategy, based on new transformation matrices (the third strategy group), is proposed for a single-phase open circuit fault. The strategy can generate a constant torque regardless of multi-harmonics in NS-EMFs. Therefore, it can be called Robust Control Approach (RCA). To avoid the control of varying reference currents, a new control scheme using a specific online-trained ADALINE is proposed. The ADALINE is based on the knowledge of rotor position and NS-EMF harmonic rank. It is used to extract amplitudes and phase angles of torque-producing harmonics in measured phase currents. Thus, time-constant feedback signals for the PI controllers are obtained. Notably, the proposed ADALINE-based control scheme with RCA can solve all problems caused by varying reference currents as previously discussed in the three strategy groups.

A 7-phase PMSM with multi-harmonics in NS-EMFs is used to verify the proposed strategy and scheme. The scheme is numerically and experimentally compared with the conventional Rotor Field-Oriented Control (RFOC) scheme. Five comparative cases are described in Table I for thorough evaluations of the proposed strategy and control scheme. Because of being used in healthy mode (case 1), the RFOC scheme is called the pre-fault control scheme. In post-fault operation, the pre-fault control scheme is preserved with strategies Maximum Torque Per Ampere (MTPA) [7, 8] (case 3) and RCA (case 4). In the pre-fault scheme, both MTPA and RCA have varying reference d-q currents. However, RCA can be used in the proposed control scheme with constant reference d-q currents (case 5), allowing to keep the PI controllers. A demonstration video is provided with this paper.

The paper is organized as follows. Section II presents the modeling and control of a 7-phase drive in healthy mode. Proposed strategy RCA is described in section III. The pre-fault and proposed control schemes are explained in sections IV and V, respectively. Numerical and experimental results are described in section VI.

II. MODELING AND CONTROL OF A SEVEN-PHASE PMSM IN HEALTHY MODE

In this study, a 7-phase PMSM with NS-EMFs is considered with several assumptions for the modelling as follows: apart from the main 1st harmonic (H1, 100%), the NS-EMFs have a significant proportion of the 3rd harmonic (H3, 32.3%) and a

small but unneglectable proportion of the 9th harmonic (H9, 12.5%); 7 phase windings are equally shifted and star-connected; the magnet circuit saturation is not considered in calculations of NS-EMFs and fluxes. The voltage and electromagnetic torque of the machine can be expressed as:

$$\underline{v} = R_s \underline{i} + [\boldsymbol{L}]\frac{\mathrm{d}\underline{i}}{\mathrm{d}t} + \Omega \underline{e}_{nor} \tag{1}$$

$$T_{em} = \underline{e}_{nor}^{\mathrm{T}} \underline{i} \tag{2}$$

with $\underline{v} = [v_A\ v_B\ v_C\ v_D\ v_E\ v_F\ v_G]^{\mathrm{T}}$; $\underline{i} = [i_A\ i_B\ i_C\ i_D\ i_E\ i_F\ i_G]^{\mathrm{T}}$;

$\underline{e}_{nor} = [e_A\ e_B\ e_C\ e_D\ e_E\ e_F\ e_G]^{\mathrm{T}}$

where $\underline{v}$, $\underline{i}$, and $\underline{e}_{nor}$ are 7-dimensional vectors of phase voltages, phase currents, and speed-normalized NS-EMFs, respectively; R_s is the resistance of one phase of the stator; $[\boldsymbol{L}]$ is a 7-by-7 stator inductance matrix; Ω is the rotating speed of rotor; T_{em} is the electromagnetic torque of the machine.

The speed-normalized NS-EMF of one phase (e_A, e_B, e_C, e_D, e_E, e_F, or e_G) is given by:

$$e_j = \sum_h E_h \sin\left\{h\left[\theta - (j-1)\frac{2\pi}{7}\right] + \varphi_h\right\} \tag{3}$$

with $h \in \{1,\ 3,\ 9\}$ and $j \in [1, 7]$

where j represents the phase number corresponding to seven phases from A to G; E_h and φ_h are the speed-normalized amplitude and phase shift angle of harmonic h, respectively; θ is the electrical position.

To facilitate RFOC as presented in [4, 5], the classical 7-by-7 transformation matrices, Clarke $[\boldsymbol{T}_{classic}]$ and Park $[\boldsymbol{P}_{classic}]$, are applied to convert parameters of the machine from natural frame into decoupled d-q frames. For example, the transformation for currents is presented as

$$[i_{d1}\ i_{q1}\ i_{d9}\ i_{q9}\ i_{d3}\ i_{q3}\ i_z]^{\mathrm{T}} = [\boldsymbol{P}_{classic}][\boldsymbol{T}_{classic}][i_A\ i_B\ i_C\ i_D\ i_E\ i_F\ i_G]^{\mathrm{T}} \tag{4}$$

Thus, a 7-phase machine can be mathematically decomposed into 3 two-phase fictitious machines (FMs) and 1 zero-sequence machine (ZM) with corresponding reference frames [31]. One FM and its reference frame are associated with a given group of harmonics as described in Table II.

The RFOC scheme, called the pre-fault control scheme in this study, is described in Fig. 2. In healthy mode, seven optimal reference phase currents $\underline{i}_{ref}$ are calculated from reference torque T_{em_ref} by using MTPA [7, 8] as

$$\underline{i}_{ref} = \frac{\underline{e}_{nor}}{\|\underline{e}_{nor}\|^2} T_{em\_ref} \tag{5}$$

TABLE II
FICTITIOUS MACHINES, REFERENCE FRAMES, AND ASSOCIATED HARMONICS OF A 7-PHASE MACHINE (ONLY ODD HARMONICS)

Fictitious machine	Frame	Associated harmonic $m \in \mathbb{N}_0$
1st two-phase machine (FM1)	d_1-q_1	$\underline{1}$, 13, …, $7m \pm 1$
2nd two-phase machine (FM2)	d_9-q_9	5, $\underline{9}$, …, $7m \pm 2$
3rd two-phase machine (FM3)	d_3-q_3	$\underline{3}$, 11, …, $7m \pm 3$
Zero-sequence machine (ZM)	z	7, 21, …, $7m$

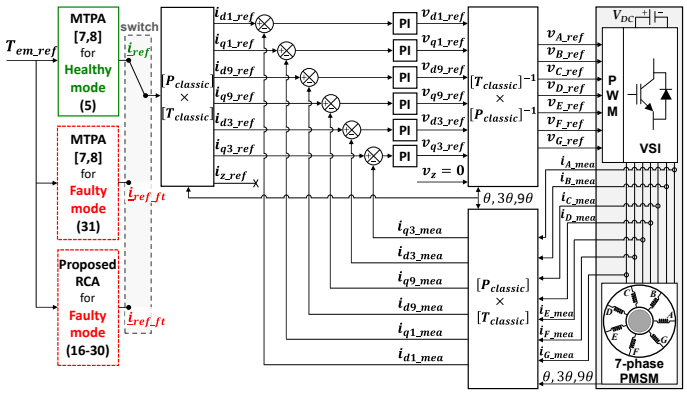

Fig. 2. RFOC scheme for torque control (called "pre-fault control scheme").

where $\|\underline{e}_{nor}\|$ is the norm of vector $\underline{e}_{nor}$. A constant torque can be generated by constant d-q currents if each two-phase fictitious machine contains only one harmonic of NS-EMFs.

The selection of a harmonic of currents in each frame for control depends on the main harmonics of NS-EMFs. A constant torque is produced by using simultaneously three harmonics: the 1st for FM1, the 9th for FM2, and the 3rd for FM3. Therefore, 6 constant d-q currents (i_{d1_ref}, i_{q1_ref}, i_{d9_ref}, i_{q9_ref}, i_{d3_ref}, i_{q3_ref}) are controlled by 6 conventional PI controllers (i_{z_ref} is always zero due to the star connection).

III. PROPOSED POST-FAULT REFERENCE CURRENTS WITH RCA

A. Reduced-order transformation matrices

When phase A, for example, is opened, i_A becomes zero. Therefore, the first column of the classical Clarke transformation matrix in [4], associated with phase A, should be removed. The classical Clarke matrix in the post-fault condition for 7-phase machines can be written with only 6 columns as follows:

$$[\boldsymbol{T}_{fault}] = \sqrt{\frac{2}{7}} \begin{bmatrix} \cos(\delta) & \cos(2\delta) & \cos(3\delta) & \cos(4\delta) & \cos(5\delta) & \cos(6\delta) \\ \sin(\delta) & \sin(2\delta) & \sin(3\delta) & \sin(4\delta) & \sin(5\delta) & \sin(6\delta) \\ \cos(2\delta) & \cos(4\delta) & \cos(6\delta) & \cos(8\delta) & \cos(10\delta) & \cos(12\delta) \\ \sin(2\delta) & \sin(4\delta) & \sin(6\delta) & \sin(8\delta) & \sin(10\delta) & \sin(12\delta) \\ \cos(3\delta) & \cos(6\delta) & \cos(9\delta) & \cos(12\delta) & \cos(15\delta) & \cos(18\delta) \\ \sin(3\delta) & \sin(6\delta) & \sin(9\delta) & \sin(12\delta) & \sin(15\delta) & \sin(18\delta) \\ \sqrt{1/2} & \sqrt{1/2} & \sqrt{1/2} & \sqrt{1/2} & \sqrt{1/2} & \sqrt{1/2} \end{bmatrix} \tag{6}$$

where $\delta = 2\pi/7$ is the spatial phase shift angle.

In (6), the first, third and fifth row vectors are no longer orthogonal to each other. Three reference frames (d_1-q_1), (d_9-q_9), and (d_3-q_3), decoupled in healthy mode, become coupled in faulty mode. Consequently, currents cannot be properly controlled without any reconfigurations. The post-fault 7-phase machine can be considered as an asymmetrical 6-phase machine with 6-by-6 transformation matrices. Therefore, the relationship between new currents in natural frame (i_{B1}, i_{C1}, i_{D1}, i_{E1}, i_{F1}, i_{G1}) and in d-q frames (i_{d11}, i_{q11}, i_{d91}, i_{q91}, i_{x1}, i_{z1}) can be represented through 6-by-6 transformation matrices as

$$[i_{B1}\ i_{C1}\ i_{D1}\ i_{E1}\ i_{F1}\ i_{G1}]^{\mathrm{T}} = [\boldsymbol{T}_1]^{-1}[\boldsymbol{P}_1]^{-1}[i_{d11}\ i_{q11}\ i_{d91}\ i_{q91}\ i_{x1}\ i_{z1}]^{\mathrm{T}} \tag{7}$$

$$[\boldsymbol{T}_1] = \sqrt{\frac{2}{7}} \begin{bmatrix} (\cos(\delta)-1) & (\cos(2\delta)-1) & (\cos(3\delta)-1) & (\cos(4\delta)-1) & (\cos(5\delta)-1) & (\cos(6\delta)-1) \\ \sin(\delta) & \sin(2\delta) & \sin(3\delta) & \sin(4\delta) & \sin(5\delta) & \sin(6\delta) \\ \cos(2\delta) & \cos(4\delta) & \cos(6\delta) & \cos(8\delta) & \cos(10\delta) & \cos(12\delta) \\ \sin(2\delta) & \sin(4\delta) & \sin(6\delta) & \sin(8\delta) & \sin(10\delta) & \sin(12\delta) \\ \sin(3\delta) & \sin(6\delta) & \sin(9\delta) & \sin(12\delta) & \sin(15\delta) & \sin(18\delta) \\ \sqrt{1/2} & \sqrt{1/2} & \sqrt{1/2} & \sqrt{1/2} & \sqrt{1/2} & \sqrt{1/2} \end{bmatrix} \tag{8}$$

$$[\boldsymbol{P_1}]=\begin{bmatrix} \cos(\theta+\varphi_1) & \sin(\theta+\varphi_1) & 0 & 0 & 0 & 0 \\ -\sin(\theta+\varphi_1) & \cos(\theta+\varphi_1) & 0 & 0 & 0 & 0 \\ 0 & 0 & 1 & 0 & 0 & 0 \\ 0 & 0 & 0 & 1 & 0 & 0 \\ 0 & 0 & 0 & 0 & 1 & 0 \\ 0 & 0 & 0 & 0 & 0 & 1 \end{bmatrix} \tag{9}$$

where $[\boldsymbol{T_1}]$ and $[\boldsymbol{P_1}]$ are new 6-by-6 Clarke and Park matrices in (8) and (9), respectively; φ_1 is the phase shift angle of the 1st harmonic of NS-EMFs as previously described in (3).

The subscript 1 in all variables of (7) means that the fundamental components of currents are being considered. Frames (d_{11}-q_{11}) and (d_{91}-q_{91}) represent 2 two-phase fictitious machines while x_1 and z_1 represent 2 zero-sequence machines. For simplicity, d-axis current i_{d11} is zero. Due to the star connection, i_{z1} is zero.

New Clarke matrix $[\boldsymbol{T_1}]$ is determined from $[\boldsymbol{T_{fault}}]$ in (6) by removing its fifth row because this row vector is not orthogonal to the first and third row vectors, and (d_3-q_3) frame in healthy mode becomes x_1 in faulty mode. In addition, coefficient -1 is added to the first row of $[\boldsymbol{T_{fault}}]$ to respect the orthogonal property between row vectors. After these modifications, the row vectors of the new matrix $[\boldsymbol{T_1}]$ in (8) are orthogonal to each other, allowing to control independently currents in the new decoupled d-q frames.

The generated torque is constant if S-EMFs are considered as in [12-19]. However, in this study, the considered NS-EMFs consist of extra harmonics, including 3rd and 9th as described in (3). Therefore, from (2)-(3) and (7)-(9), the electromagnetic torque T_{em1}, obtained with only sinusoidal currents, can be generally described as

$$\begin{aligned} T_{em1} = T_{ave1} &+ E_3 i_{q11}\{f_1(2\theta)+f_2(4\theta)\} + E_9 i_{q11}\{f_3(8\theta)+f_4(10\theta)\} \\ &+ \underline{e}^{\mathrm{T}}_{nor\_ft}\left\{[\boldsymbol{K_1}]\begin{bmatrix} i_{d91} & i_{q91} & i_{x1}\end{bmatrix}^{\mathrm{T}}\right\} \end{aligned} \tag{10}$$

$$\text{with } T_{ave1} = \sqrt{7/2}E_1 i_{q11}\,;$$

$$\underline{e}_{nor\_ft} = [e_B\ e_C\ e_D\ e_E\ e_F\ e_G]^{\mathrm{T}} = \underline{e}_{nor\_ft1} + \underline{e}_{nor\_ft3} + \underline{e}_{nor\_ft9}$$

where T_{ave1} is the average torque; E_1, E_3, and E_9 are respectively the amplitudes of the 1st, 3rd, and 9th harmonics of a speed-normalized NS-EMF in (3); f_1, f_2, f_3, and f_4 are trigonometric functions of harmonics 2θ, 4θ, 8θ, and 10θ, respectively; $\underline{e}_{nor\_ft}$ is a 6-dimensional vector derived from $\underline{e}_{nor}$ in (1)-(2) by removing e_A; $\underline{e}_{nor\_ft1}$, $\underline{e}_{nor\_ft3}$, and $\underline{e}_{nor\_ft9}$ are 6-dimensional vectors derived by preserving only the 1st, or 3rd, or 9th harmonic in $\underline{e}_{nor\_ft}$, respectively; $[\boldsymbol{K_1}]$ is a constant 6-by-3 matrix obtained from the 3rd to 5th columns of $[\boldsymbol{T_1}]^{-1}$.

In (10), the harmonics of the torque are generated by interactions between the fundamental components of currents and the harmonics of the NS-EMFs. Terms f_3 and f_4 caused by the fundamental current and the 9th harmonic of NS-EMFs are nullified due to the chosen matrices, leading to an expression of the torque as

$$\begin{aligned} T_{em1} = T_{ave1} &+ E_3 i_{q11}\{f_1(2\theta)+f_2(4\theta)\} \\ &+ \underline{e}^{\mathrm{T}}_{nor\_ft}\left\{[\boldsymbol{K_1}]\begin{bmatrix} i_{d91} & i_{q91} & i_{x1}\end{bmatrix}^{\mathrm{T}}\right\} \end{aligned} \tag{11}$$

In (11), by simply imposing currents (i_{d91}, i_{q91}, i_{x1}) to be zero, torque ripples caused by harmonics of $\underline{e}_{nor\_ft}$ can be eliminated. However, torques with frequencies 2θ and 4θ cannot be eliminated due to the 3rd harmonic of NS-EMFs with amplitude E_3 and constant current i_{q11}.

It will be seen that the injection of the 3rd harmonic components of currents allows to compensate the pulsating torques 2θ and 4θ. Indeed, the 3rd harmonic components of currents in natural frame (i_{B3}, i_{C3}, i_{D3}, i_{E3}, i_{F3}, i_{G3}) are calculated from new d-q currents (i_{x3}, i_{d93}, i_{q93}, i_{d33}, i_{q33}, i_{z3}) as follows:

$$[i_{B3}\ i_{C3}\ i_{D3}\ i_{E3}\ i_{F3}\ i_{G3}]^{\mathrm{T}} = [\boldsymbol{T_3}]^{-1}[\boldsymbol{P_3}]^{-1}[i_{x3}\ i_{d93}\ i_{q93}\ i_{d33}\ i_{q33}\ i_{z3}]^{\mathrm{T}} \tag{12}$$

$$[\boldsymbol{T_3}]=\sqrt{\frac{2}{7}}\begin{bmatrix} \sin(\delta) & \sin(2\delta) & \sin(3\delta) & \sin(4\delta) & \sin(5\delta) & \sin(6\delta) \\ \cos(2\delta) & \cos(4\delta) & \cos(6\delta) & \cos(8\delta) & \cos(10\delta) & \cos(12\delta) \\ \sin(2\delta) & \sin(4\delta) & \sin(6\delta) & \sin(8\delta) & \sin(10\delta) & \sin(12\delta) \\ (\cos(3\delta)-1) & (\cos(6\delta)-1) & (\cos(9\delta)-1) & (\cos(12\delta)-1) & (\cos(15\delta)-1) & (\cos(18\delta)-1) \\ \sin(3\delta) & \sin(6\delta) & \sin(9\delta) & \sin(12\delta) & \sin(15\delta) & \sin(18\delta) \\ \sqrt{1/2} & \sqrt{1/2} & \sqrt{1/2} & \sqrt{1/2} & \sqrt{1/2} & \sqrt{1/2} \end{bmatrix} \tag{13}$$

$$[\boldsymbol{P_3}]=\begin{bmatrix} 1 & 0 & 0 & 0 & 0 & 0 \\ 0 & 1 & 0 & 0 & 0 & 0 \\ 0 & 0 & 1 & 0 & 0 & 0 \\ 0 & 0 & 0 & \cos(3\theta+\varphi_3) & \sin(3\theta+\varphi_3) & 0 \\ 0 & 0 & 0 & -\sin(3\theta+\varphi_3) & \cos(3\theta+\varphi_3) & 0 \\ 0 & 0 & 0 & 0 & 0 & 1 \end{bmatrix} \tag{14}$$

where $[\boldsymbol{T_3}]$ and $[\boldsymbol{P_3}]$ are new 6-by-6 Clarke and Park matrices as presented in (13) and (14), respectively; φ_3 is the phase shift angle of the 3rd harmonic of NS-EMFs as described in (3).

Like (7), the subscript 3 in all variables of (12) means that the third harmonic components of currents are being considered. Frames (d_{93}-q_{93}) and (d_{33}-q_{33}) represent 2 two-phase fictitious machines while x_3 and z_3 represent 2 zero-sequence machines. For simplicity, d-axis current i_{d33} is set to zero. Besides, the zero-sequence current i_{z3} is zero due to the star connection. Similar to $[\boldsymbol{T_1}]$, 6-by-6 matrix $[\boldsymbol{T_3}]$ in (13) is defined from matrix $[\boldsymbol{T_{fault}}]$ in (6) by eliminating its first row because this row vector is not orthogonal to the third and fifth row vectors, and (d_1-q_1) frame in healthy mode becomes x_3 in faulty mode. In addition, coefficient -1 is added to the fifth row of $[\boldsymbol{T_{fault}}]$ due to the requirement of orthogonality. As a result, the orthogonal property of row vectors in $[\boldsymbol{T_3}]$ enables to control independently currents in new decoupled d-q frames.

From (2)-(3) and (7)-(14), the electromagnetic torque T_{em13}, obtained with non-sinusoidal currents, is expressed as

$$\begin{aligned} T_{em13} = T_{ave13} &+ \{E_3 i_{q11} + E_1 i_{q33}\}\{f_1(2\theta)+f_2(4\theta)\} \\ &+ \{E_3 i_{q33} + E_9 i_{q33}\} f_5(6\theta) + E_9 i_{q33} f_6(12\theta) \\ &+ \underline{e}^{\mathrm{T}}_{nor\_ft}\left\{[\boldsymbol{K_1}]\begin{bmatrix} i_{d91} & i_{q91} & i_{x1}\end{bmatrix}^{\mathrm{T}} + [\boldsymbol{K_3}]\begin{bmatrix} i_{x3} & i_{d93} & i_{q93}\end{bmatrix}^{\mathrm{T}}\right\} \end{aligned} \tag{15}$$

$$\text{with } T_{ave13} = \sqrt{7/2}\left(E_1 i_{q11} + E_3 i_{q33}\right)$$

where T_{ave13} is the average torque with the additional third harmonic components; f_5 and f_6 are trigonometric functions of harmonics 6θ and 12θ, respectively; $[\boldsymbol{K_3}]$ is a constant 6-by-3 matrix obtained from the 1st to 3rd columns of $[\boldsymbol{T_3}]^{-1}$.

In (15), f_5 and f_6 caused by the 3rd harmonic current and the 3rd and 9th harmonics of NS-EMFs are nullified due to the chosen matrices. In addition, to eliminate torque ripples at

frequencies of 2θ and 4θ, current i_{q33} in (15) needs to be calculated as

$$i_{q33} = -(E_3 / E_1) i_{q11} \tag{16}$$

Simultaneously, the effect of the 1st and 3rd harmonics of NS-EMFs ($\underline{e}_{nor\_ft1}$ and $\underline{e}_{nor\_ft3}$ in $\underline{e}_{nor\_ft}$) in the last term of (15) is also eliminated. Finally, the electromagnetic torque is calculated with an impact of the 9th harmonic of NS-EMFs $\underline{e}_{nor\_ft9}$ as follows:

$$\begin{aligned} T_{em13} &= T_{ave13} + \\ &+ \underline{e}_{nor\_ft9}^{\mathrm{T}} \left\{ [\boldsymbol{K_1}] \begin{bmatrix} i_{d91} & i_{q91} & i_{x1} \end{bmatrix}^{\mathrm{T}} + [\boldsymbol{K_3}] \begin{bmatrix} i_{x3} & i_{d93} & i_{q93} \end{bmatrix}^{\mathrm{T}} \right\} \end{aligned} \tag{17}$$

$$\text{with } T_{ave13} = \sqrt{7/2}\left[E_1 i_{q11} + E_3 i_{q33}\right] = \sqrt{7/2}\left[\left(E_1^2 - E_3^2\right)/E_1\right] i_{q11}$$

B. Robust Control Approach (RCA) for new reference currents

From (15)-(17), (i_{q11}, i_{q33}) are imposed as constants to generate the average torque while currents (i_{d11}, i_{d33}) are zero. If six currents (i_{d91}, i_{q91}, i_{x1}) and (i_{x3}, i_{d93}, i_{q93}) are imposed to be zero, the electromagnetic torque T_{em13} in (17) is constant and equal to the average torque T_{ave13} as

$$T_{em13} = T_{ave13} = \sqrt{7/2}\left[E_1 i_{q11} + E_3 i_{q33}\right] = \sqrt{7/2}\left[\left(E_1^2 - E_3^2\right)/E_1\right] i_{q11} \tag{18}$$

From (7)-(9), the 1st harmonic components of reference currents in the six remaining healthy phases are calculated from currents in d-q frames as follows:

$$i_{B1} = 0.9158 i_{q11} \sin(\theta + 152.8^0 + \varphi_1) \tag{19}$$

$$i_{C1} = 0.6899 i_{q11} \sin(\theta + 49^0 + \varphi_1) \tag{20}$$

$$i_{D1} = 0.4304 i_{q11} \sin(\theta + 32.6^0 + \varphi_1) \tag{21}$$

$$i_{E1} = 0.4304 i_{q11} \sin(\theta - 32.6^0 + \varphi_1) \tag{22}$$

$$i_{F1} = 0.6899 i_{q11} \sin(\theta - 49^0 + \varphi_1) \tag{23}$$

$$i_{G1} = 0.9158 i_{q11} \sin(\theta - 152.8^0 + \varphi_1) \tag{24}$$

Calculations for (i_{B3}, i_{C3}, i_{D3}, i_{E3}, i_{F3}, i_{G3}) are similar by using (12)-(14) as

$$i_{B3} = 0.8473 i_{q33} \sin(3\theta + 15.9^0 + \varphi_3) \tag{25}$$

$$i_{C3} = 0.6157 i_{q33} \sin(3\theta - 137.3^0 + \varphi_3) \tag{26}$$

$$i_{D3} = 0.6348 i_{q33} \sin(3\theta + 124.8^0 + \varphi_3) \tag{27}$$

$$i_{E3} = 0.6348 i_{q33} \sin(3\theta - 124.8^0 + \varphi_3) \tag{28}$$

$$i_{F3} = 0.6157 i_{q33} \sin(3\theta + 137.3^0 + \varphi_3) \tag{29}$$

$$i_{G3} = 0.8473 i_{q33} \sin(3\theta - 15.9^0 + \varphi_3) \tag{30}$$

In summary, the total torque in (18) is constant and obtained by using reference currents calculated from (16) and (19)-(30). Reference currents of the six remaining healthy phases in the post-fault operation are combinations of the 1st harmonic currents in (19)-(24) and the 3rd harmonic currents in (25)-(30).

The drive using the above new reference currents (RCA) has robustness. Indeed, a constant torque can be obtained in post-fault operation with multi-harmonics in NS-EMFs (1st in FM1, 9th in FM2, and 3rd in FM3). Therefore, RCA can solve the existing problem in the first group strategies in dealing with multi-harmonics in NS-EMFs. Specifically, in [2-6], d-q currents generating most of the torque (1st and 3rd harmonics, for example) are preferred to be constant. Other d-q currents are forcedly time-variant (9th harmonic). If the corresponding NS-EMF harmonic (9th harmonic) is not null, torque ripples are inevitable. Generally, RCA can be adapted for multiphase machines with different phase numbers.

IV. Pre-fault Control Scheme In Post-fault Operation

A. Maximum Torque Per Ampere for faulty modes

Optimal currents, generating maximum constant torques with minimum copper losses, are obtained either by using the Lagrangian multipliers in [7] or by the real-time vectorial control approach in [8]. Although the two approaches are different, the obtained optimal currents in [7] and [8] are the same. These methods are called Maximum Torque Per Ampere (MTPA) for multiphase machines. Without loss of generality, the vectorial approach in [8] is presented and compared with the proposed strategy and control scheme in this paper. When phase A is opened, new reference phase currents for the six remaining healthy phases $\underline{i}_{ref\_ft}$, generating a constant reference torque T_{em_ref}, are given by [8] as

$$\underline{i}_{ref\_ft} = \frac{\underline{e}_{nor\_ft} - \underline{e}_z}{\left\| \underline{e}_{nor\_ft} - \underline{e}_z \right\|^2} T_{em\_ref} \text{ with } \underline{e}_z = \left(\sum_{j=2}^{n} e_j \right) \frac{1}{n-1} \underline{u} \tag{31}$$

where n is the number of phases; $\underline{e}_z$ is a zero-sequence speed-normalized NS-EMF vector to satisfy a null zero-sequence current in the star connection; $\underline{u}$ is the 6-dimensional unit vector; $\left\| \underline{e}_{nor\_ft} - \underline{e}_z \right\|$ is the norm of vector $\left(\underline{e}_{nor\_ft} - \underline{e}_z \right)$.

Theoretically, the optimal reference currents in (31) can generate constant torques with minimum copper losses. Especially, by using classical transformation matrices, six reference d-q currents are time-variant as shown in Fig. 3a. These varying reference currents are controlled by PI controllers of the pre-fault control scheme in Fig. 2.

B. The proposed RCA in the pre-fault control scheme

Constant reference d-q currents (i_{d11}, i_{q11}, i_{d91}, i_{q91}, i_{x1}) and (i_{x3}, i_{d93}, i_{q93}, i_{d33}, i_{q33}) from RCA can be used for control. However, it is difficult to obtain corresponding constant feedback signals for current controllers because at least the 1st and 3rd harmonics are combined in measured phase currents. In literature review, no transformation matrices have been found to obtain all constant d-q currents with post-fault multi-harmonic phase currents.

For the sake of simplicity, the pre-fault control scheme in Fig. 2 can be reused. Indeed, i_{q11} is obtained from a reference torque T_{em_ref} by using (18), and i_{q33} is then derived from (16). Thus, new reference currents for remaining healthy phases are the sums of their 1st and 3rd harmonic components in (19)-(30). Classical matrices are used to transform these new reference currents from natural frame into d-q frames for control,

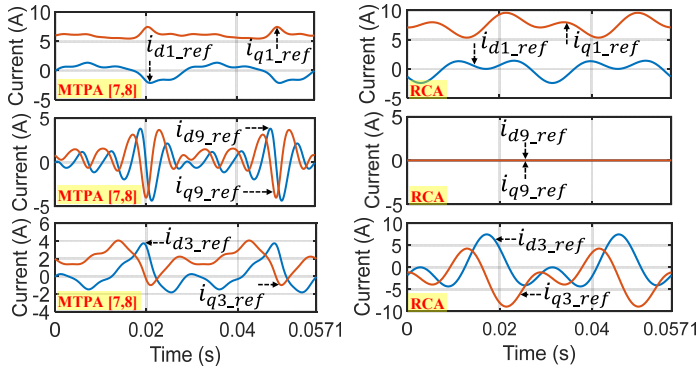

Fig. 3. (Numerical results) New post-fault reference d-q currents at 350 rpm with MTPA [7, 8] (a), and with the proposed RCA (b), for the pre-fault control scheme in Fig. 2 (at least i_{d1_ref}, i_{q1_ref}, i_{d3_ref}, and i_{q3_ref} are not constant).

resulting in varying reference d-q currents as in [22-24]. Fig. 3b shows new reference d-q currents with RCA using classical transformation matrices. Notably, RCA possesses null reference currents in (d_9-q_9) frame. Therefore, NS-EMF harmonics associated with the second fictitious machine (5th and 9th, for example) will not generate torque ripples.

V. Proposed Adaline-based Control Scheme In Post-fault Operation

A. The proposed ADALINE-based control scheme

The new control scheme for an open circuit fault in phase A, as described in Fig. 4, can directly control constant currents, facilitating current control with limited bandwidth controllers as PI. Feedback signals for current controllers can be obtained from non-sinusoidal measured phase currents. Indeed, measured phase currents and electrical position are sent to a real-time current learning (RTCL) block to determine torque-producing harmonic components of measured phase currents. From the NS-EMF assumption in this study, the 1st and 3rd harmonic components of phase currents need to be determined. Therefore, RTCL extracts harmonic components of all measured phase currents in natural frame. After that, new matrices ($[\boldsymbol{T}_1],[\boldsymbol{P}_1]$) in (7)-(9) and ($[\boldsymbol{T}_3],[\boldsymbol{P}_3]$) in (12)-(14) transform the extracted current harmonics into d-q frames to obtain necessary time-constant feedback signals for current controllers. Due to the star connection, currents (i_{z1}, i_{z3}) are always equal to zero. Thus, in the proposed control scheme, 10 PI controllers are used to control 10 constant currents (i_{d11}, i_{q11}, i_{d91}, i_{q91}, i_{x1}) and (i_{x3}, i_{d93}, i_{q93}, i_{d33}, i_{q33}). Among these 10 currents, 2 currents (i_{q11}, i_{q33}) mainly generate torque while the others are imposed to be zero.

The key part of RTCL is a specific ADALINE that is presented in the next subsection. The ADALINE extracts harmonics of the measured current of only one arbitrary healthy phase among the six remaining healthy phases. Then, the other phase currents are derived from the ADALINE-based extracted current according to RCA strategy. To sum up, from Fig. 4, there are three steps to implement RTCL as follows:

1) Extract the first and third harmonics of an arbitrary measured healthy phase current by using the ADALINE.

2) The first harmonic of this current is used to calculate the first harmonics of other phase currents by using RCA (apply (19)-(24) when phase A is opened).

3) The third harmonics of phase currents are equal to differences between measured phase currents and the corresponding first harmonics as described in RTCL of Fig. 4.

B. Descriptions of the proposed ADALINE in RTCL

Without loss of generality, the measured phase-B current i_{B_mea} is chosen for the harmonic extraction when phase A is opened. With the NS-EMF assumption, the 1st and 3rd harmonics are torque-producing components, i_{B_mea} can be expressed by Fourier coefficients as

$$\begin{aligned} i_{B\_mea} &= \left[\mu_1^* \sin(\theta) + \mu_2^* \cos(\theta)\right] + \left[\mu_3^* \sin(3\theta) + \mu_4^* \cos(3\theta)\right] \\ &= \left(\sqrt{\left(\mu_1^*\right)^2 + \left(\mu_2^*\right)^2}\right) \sin\left(\theta + arctg\left(\frac{\mu_2^*}{\mu_1^*}\right)\right) + \left(\sqrt{\left(\mu_3^*\right)^2 + \left(\mu_4^*\right)^2}\right) \sin\left(3\theta + arctg\left(\frac{\mu_4^*}{\mu_3^*}\right)\right) \end{aligned} \quad (32)$$

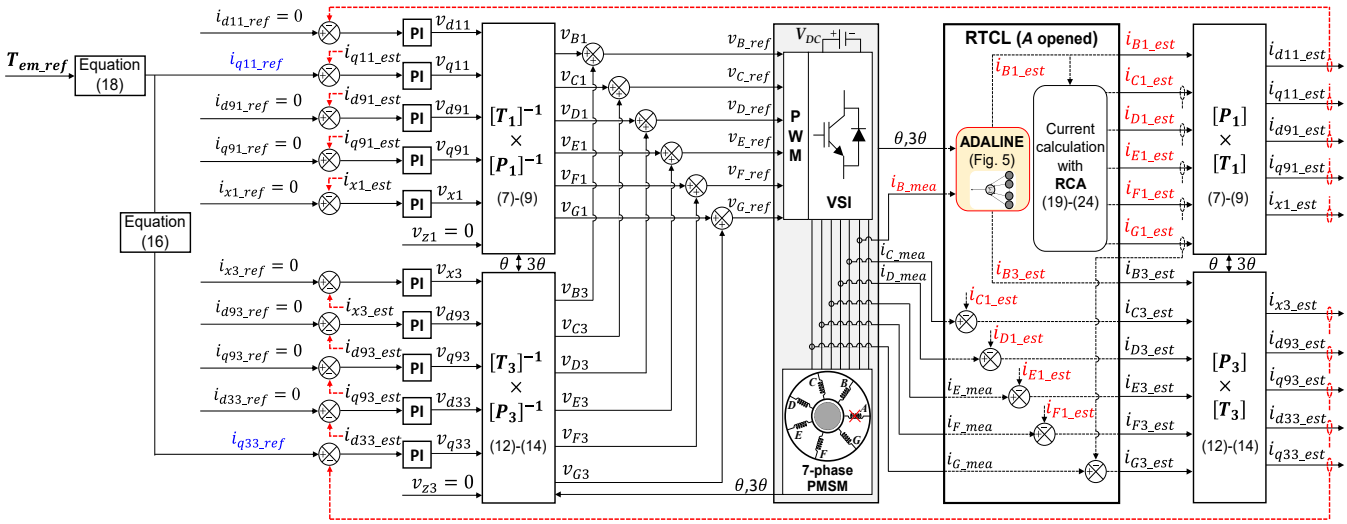

Fig. 4. Proposed ADALINE-based control scheme using RCA to control 10 constant d-q currents with PI controllers when phase A is opened.

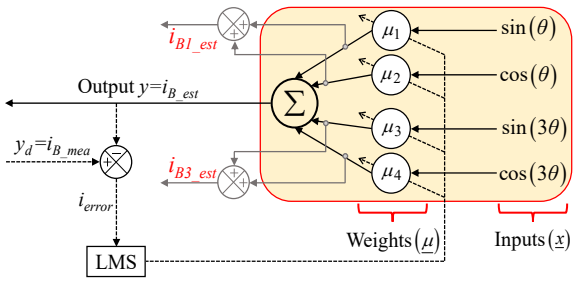

Fig. 5. Harmonic extraction of the measured phase-*B* current using an ADALINE with a single layer, for NS-EMFs with 1st and 3rd harmonics.

where μ_j^* are the coefficients of harmonic components (j=1, 2, 3, 4); θ is the electrical position measured from an encoder.

The harmonic extraction of i_{B_mea} by the proposed ADALINE is shown in Fig. 5. The input vector and the weight vector of the ADALINE are defined by:

$$\underline{x}=[\sin(\theta)\quad \cos(\theta)\quad \sin(3\theta)\quad \cos(3\theta)]^{\mathrm{T}} \tag{33}$$

$$\underline{\mu}=[\mu_1\quad \mu_2\quad \mu_3\quad \mu_4]^{\mathrm{T}} \tag{34}$$

where (μ_1, μ_2) are weights representing harmonic θ; and (μ_3, μ_4) are weights representing harmonic 3θ.

Then, the output of the ADALINE y is given by:

$$\begin{aligned} y=i_{B\_est}=i_{B1\_est}+i_{B3\_est}=\underline{\mu}^{\mathrm{T}}\underline{x}= \\ =[\mu_1\sin(\theta)+\mu_2\cos(\theta)]+[\mu_3\sin(3\theta)+\mu_4\cos(3\theta)] \end{aligned} \tag{35}$$

where i_{B_est} is the estimated current, i_{B1_est} and i_{B3_est} are the extracted first and third harmonic components of the current.

Four weights (μ_1, μ_2, μ_3, μ_4) can be updated by using iterative linear Least Mean Square (LMS) rule. Compared to other types of artificial neural networks, the ADALINE weights can be interpreted [10]. The weights are updated at each sampled time k as

$$\underline{\mu}(k+1)=\underline{\mu}(k)+\eta[y_d(k)-y(k)]\underline{x}(k)=\underline{\mu}(k)+\eta i_{error}(k)\underline{x}(k) \tag{36}$$

where η is the learning rate; y_d is the desired output (i_{B_mea}); i_{error} is the error between i_{B_mea} (y_d) and i_{B_est} (y).

The learning rate mainly depends on the sampling time in calculations and desired signal characteristics such as amplitudes. Generally, η must be between 0 and 1 to guarantee the system stability. An increase in η results in faster convergence but may lead to divergence. On each iteration, the weights are enforced to converge to the coefficients of the measured current i_{B_mea}. After a given number of iterations, the weights converge as

$$\mu_j(k)\underset{k\to\infty}{\to}\mu_j^* \text{ then } i_{B\_est}\underset{k\to\infty}{\to}i_{B\_mea} \tag{37}$$

where μ_j^* are the coefficients of the measured current given by (32). Finally, the estimated current i_{B_est} converges to the measured current i_{B_mea} to obtain extracted harmonics.

The accuracy of the ADALINE training can be evaluated by using Mean Squared Error (MSE) as

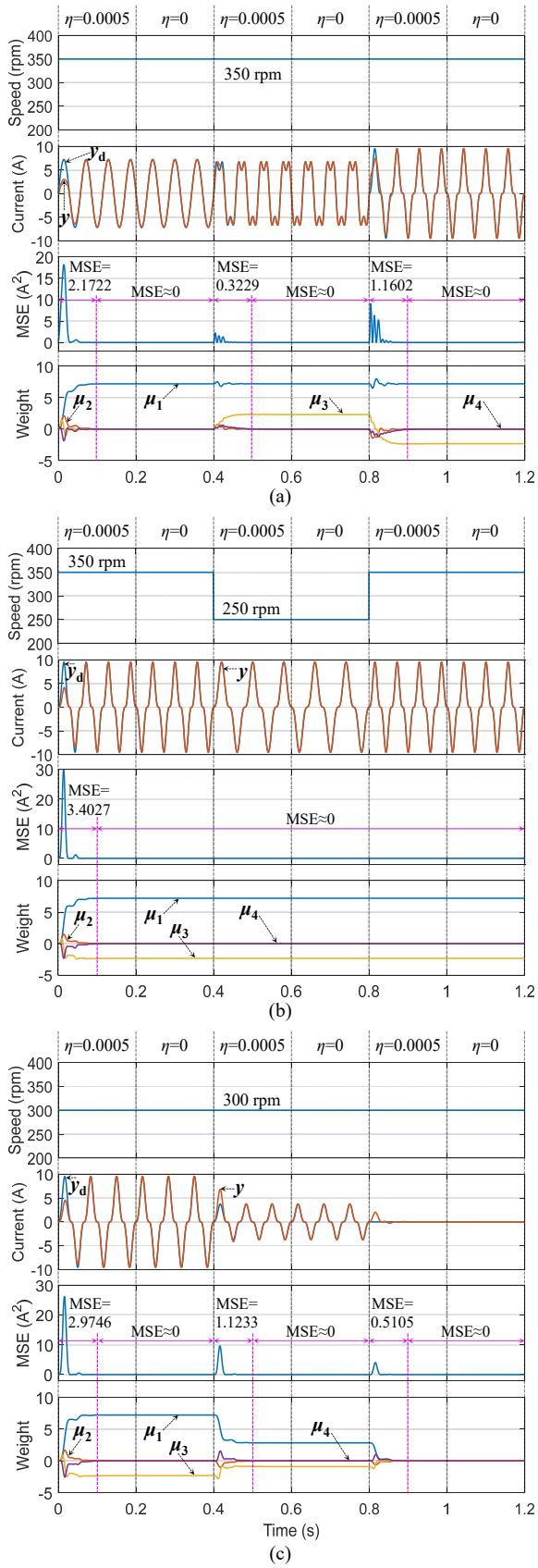

Fig. 6. (Numerical results) Validation of the proposed ADALINE with different desired current waveforms (a), with different rotating speeds (b), with different current amplitudes (representing different reference torques) (c).

$$\mathrm{MSE}=\frac{1}{N}\sum_{k=1}^{N}(y_d-y)^2=\frac{1}{N}\sum_{k=1}^{N}\left(i_{B\_mea}-i_{B\_est}\right)^2=\frac{1}{N}\sum_{k=1}^{N}i_{error}^2 \quad (38)$$

where N is the number of data points.

In this system, the knowledge of harmonics in the electric drive leads to the determination of the ADALINE inputs. The nonlinear inputs with sine and cosine functions of electrical positions θ and 3θ vary within -1 and 1. However, the relation between the input vector and the output is linear. The weights are constant in steady states, and fast convergence can be observed in transient states. Three desired current waveforms at 350 rpm are used to validate the ADALINE convergence as described in Fig. 6a. When a new current waveform is applied (at 0.4 s and 0.8 s), the learning rate must be greater than zero (η=0.0005). The transient (training) periods are less than 0.1 s (with MSE=0.3229 and MSE=1.1602). In steady states, the ADALINE output can properly track the three desired currents (MSE≈0) even when learning rate η is zero.

In Fig. 6b, rotating speed variations between 250 rpm and 350 rpm (at 0.4 s and 0.8 s) do not lead to variations in amplitudes and phase shift angles of current harmonics. Only the ADALINE trigonometric inputs vary faster or slower within -1 and 1 (electrical period variations). Thus, four weights are unchanged even when the learning rate is greater than zero in the transient periods (MSE≈0). However, variations in current amplitudes at 0.4 s and 0.8 s in Fig. 6c can represent reference torque changes in this study. In this case, the weights need to be automatically updated to obtain new values. The learning rate must be greater than zero (η=0.0005) in the transient periods (MSE=1.1233 and MSE=0.5105). In steady states (MSE≈0), the learning rate can be zero. Therefore, the proposed control scheme using the ADALINE can be applied to variable-torque and -speed applications.

Compared to conventional harmonic extraction methods such as Fast Fourier Transform, Low Pass Filters, and Phase-Locked Loop, the ADALINE possesses several outstanding advantages such as self-learning, fast convergence, and simple implementation [10, 28-30]. The use of a single ADALINE in the proposed control scheme can avoid the calculation burden, allowing RTCL to be easily implemented in real-time systems. In this study, the S-function builder in MATLAB Simulink is used to implement the ADALINE.

VI. Numerical And Experimental Verification

A. Descriptions of the experimental test bench

The proposed fault-tolerant control scheme with RCA is tested with an experimental 7-phase test bench as described in Fig. 7a and Table III. A 7-phase PMSM is supplied by 7 legs of a 12-leg voltage source inverter (VSI) using IGBTs. The VSI is fed by a DC-bus voltage in parallel to a programmable resistive load to absorb the regenerative energy. The two-level single modulation carrier-based Pulse Width Modulation (PWM) strategy with a frequency of 10 kHz is used to generate switching signals for IGBTs. A dSPACE 1005 processor is used to execute the algorithm. The dSPACE I/O boards transmit the switching signals to the VSI, receive the rotor

Table III
Electrical Parameters Of Experimental 7-phase PMSM Drive

Parameter	Unit	Value
Stator resistance R_s	Ω	1.4
Self-inductance L	mH	14.7
Mutual inductance M_1	mH	3.5
Mutual inductance M_2	mH	-0.9
Mutual inductance M_3	mH	-6.1
The 1st harmonic of speed-normalized NS-EMFs E_1	V/rad/s	1.27
Number of pole pairs p		3
Rated RMS current	A	5.1
Rated torque	N·m	32
Rated speed	rpm	750
Rated power	kW	2.5
Rated voltage	V	113
Maximum DC-bus voltage V_{DC}	V	200
PWM frequency	kHz	10

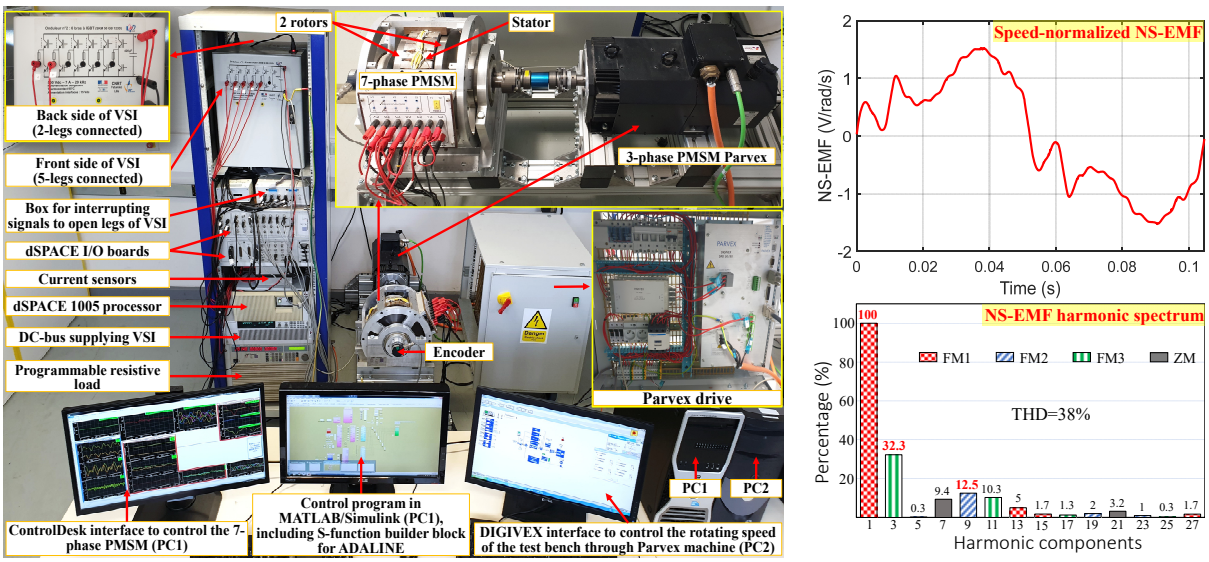

(a) (b)

Fig. 7. Experimental 7-phase drive test bench (a), and an experimental speed-normalized NS-EMF with its harmonic spectrum in the 7-phase PMSM (b).

position signal from an encoder, and receive phase current signals from current sensors. In computer PC1, MATLAB/Simulink is used for programming, including the S-function builder block for the ADALINE. When this MATLAB program is compiled, the 7-phase drive is controlled through a dSPACE control interface, namely ControlDesk (also in PC1). To create an open-circuit fault in a phase, an interrupting signal from ControlDesk is sent to the VSI to open simultaneously two IGBTs of the related phase (leg) of the inverter, disconnecting this phase from the power source. Notably, the 7-phase PMSM is mechanically connected to an industrial 3-phase PMSM ("Parvex") as a load machine. The load machine drive is used to independently adjust the speed of the 7-phase test bench by using a control interface, namely DIGIVEX, installed in computer PC2.

In Fig. 7a, the axial-flux 7-phase PMSM has two rotors respectively with 6 poles and 18 poles. Its electrical parameters are described in Table III. An experimental speed-normalized NS-EMF of one phase and its harmonic spectrum with THD=38% are shown in Fig. 7b. Specifically, the 1st and 3rd harmonics accounting for the highest proportions (100% H1, 32.3% H3), are exploited to generate the average torque. Meanwhile, the 9th harmonic (12.5% H9) is considered as a disturbance, generating torque ripples in degraded mode. Moreover, the experimental NS-EMF consists of other harmonics with minor proportions, for example, the 7th, 11th, and 13th harmonics.

With such a NS-EMF, keeping smooth torque in normal and faulty modes is challenging, especially alongside the additional requirement to keep simple PI controllers as the heart of the control. Due to the presence of three harmonics, the waveforms of currents are complex in natural frame (Fig. 8b and Fig. 10) even if they are constant in d-q frames.

Generally, to evaluate torque quality in this study, torque ripple ΔT can be calculated as

$$\Delta T = \frac{max(T_{em}) - min(T_{em})}{T_{ave}} 100\% \tag{39}$$

where *max* and *min* are functions to obtain maximum and minimum values of the instantaneous torque T_{em}, respectively; T_{ave} is the average torque.

B. Numerical results

In this study, numerical results including calculated and simulated results are obtained by considering only 1st, 3rd, and 9th harmonics in NS-EMFs. The calculated results are directly obtained from reference currents. Therefore, calculated post-fault torques by either MTPA [7, 8] or the proposed RCA are constant. Meanwhile, the simulated results are derived from the drive model in MATLAB Simulink with PI controllers for currents. Five operating stages, corresponding to five cases presented in Table I, are used for validation as follows:

1) Stage 1: Optimal currents in (5) with MTPA [7, 8] are used for healthy mode in the pre-fault control scheme (Fig. 2). Hence, six constant reference d-q currents are used for control.

2) Stage 2: An open-circuit fault happens in phase *A* without any reconfigurations. The current of phase *A* becomes zero.

3) Stage 3: The pre-fault control scheme is preserved, and new varying reference d-q currents (Fig. 3a) with MTPA [7, 8] are imposed.

4) Stage 4: The pre-fault control scheme is preserved, new reference d-q currents (Fig. 3b) by the proposed RCA are imposed.

5) Stage 5: The proposed ADALINE-based control scheme with RCA (Fig. 4) is applied to facilitate control of constant reference d-q currents.

To respect the rated RMS current 5.1 A of the considered PMSM in all operating stages, a reference torque of 15.9 N.m is chosen. In Fig. 8a, simulated torques in the five operating stages at 100 rpm, 350 rpm, and 750 rpm are described. At 100 rpm, torque quality by MTPA (stage 3) and by RCA (stages 4 and 5) is not significantly different (5.3% to 7.5%). Thus, at low frequency, PI controllers are sufficient. Meanwhile, at 350 rpm, simulated torque ripples in stages 3 and 4 using the pre-fault control scheme (14.8% and 12.7%, respectively) are much higher than that of stage 5 (8%). At this speed, PI controllers cannot properly track varying reference currents (Fig. 3) in stages 3 and 4. Meanwhile, in stage 5, constant reference currents are used for control in the proposed control scheme (learning rate η=0.0001).

Interestingly, the effectiveness of the proposed ADALINE-based control scheme becomes clearer at higher speeds (a torque ripple of 8.6 % in stage 5 compared to 17 % in stages 3 and 4 at 750 rpm). The numerical post-fault torques in stages 3 to 5 at 100 rpm, 350 rpm, and 750 rpm are summarized in

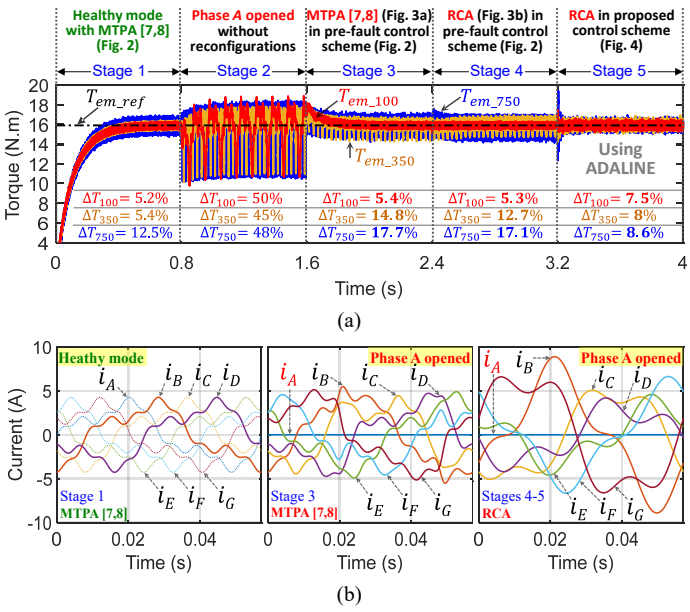

Fig. 8. (Numerical results) Simulated torques in 5 operating stages at 100 rpm (red), 350 rpm (yellow), and 750 rpm (blue) (a), calculated reference phase currents at 350 rpm with MTPA [7, 8] in healthy mode (stage 1), with MTPA [7, 8] in faulty mode (stage 3), and with the proposed RCA in faulty mode (stages 4 and 5) (b).

TABLE IV
NUMERICAL AND EXPERIMENTAL TORQUE RIPPLES WITH NEW REFERENCE CURRENTS BY MTPA [7, 8] AND RCA WHEN PHASE *A* IS OPENED

Operating speed Ω (rpm)	Stage 3*			Stage 4*			Stage 5**		
	ΔT with MTPA [7, 8] (%)			ΔT with RCA (%)			ΔT with RCA (%)		
	cal	*sim*	*exp*	*cal*	*sim*	*exp*	*cal*	*sim*	*exp*
100	0	5.4	18.1	0	5.3	12.9	0	7.5	15.9
350	0	14.8	36	0	12.7	27.9	0	8	18.5
750	0	17.7	-	0	17.1	-	0	8.6	-

cal: calculated; *sim*: simulated; *exp*: experimental.
* Using the pre-fault control scheme (Fig. 2).
** Using the proposed ADALINE-based control scheme (Fig. 4).

TABLE V
NUMERICAL AND EXPERIMENTAL COPPER LOSSES WITH NEW REFERENCE CURRENTS BY MTPA [7, 8] AND RCA WHEN PHASE *A* IS OPENED AT 350 RPM

Phase	Stage 3*			Stage 4*			Stage 5**		
	P_{loss} with MTPA (*pu*)			P_{loss} with RCA (*pu*)			P_{loss} with RCA (*pu*)		
	cal	*sim*	*exp*	*cal*	*sim*	*exp*	*cal*	*sim*	*exp*
B	1.88	1.87	1.88	4.45	4.37	3.92	4.45	4.45	4.82
C	1.43	1.36	1.31	2.52	2.20	1.74	2.52	2.49	2.68
D	1.30	1.29	1.26	1.11	1.39	1.48	1.11	1.1	1.03
E	1.29	1.23	1.23	1.11	1.08	0.98	1.11	1.1	1.16
F	1.21	1.24	1.25	2.52	2.27	2.30	2.52	2.50	2.36
G	1.65	1.66	1.64	4.45	4.07	4.03	4.45	4.40	4.21
$P_{loss\ total}$	**1.25**	**1.24**	**1.23**	**2.30**	**2.20**	**2.10**	**2.30**	**2.30**	**2.32**

cal: calculated; *sim*: simulated; *exp*: experimental.
* Using the pre-fault control scheme (Fig. 2).
** Using the proposed ADALINE-based control scheme (Fig. 4).

Table IV. In the pre-fault scheme, RCA has slightly lower torque ripples compared to MTPA. Indeed, all reference d-q currents by MTPA (Fig. 3a) are not constant with high frequency oscillations while RCA has 2 constant reference currents (i_{d9}=i_{q9}=0) (Fig. 3b).

To generate the same average torque, calculated remaining healthy phase currents with RCA (stages 4 and 5) have a higher maximum peak value compared to MTPA (stage 3) and healthy mode (stage 1) as presented in Fig. 8b. Numerical post-fault copper losses (stages 3 to 5) compared to those of healthy mode (stage 1) are summarized in Table V. Per unit (*pu*) based on parameters of healthy mode is applied to evaluate changes of parameters in the post-fault operation over healthy mode. The calculated and simulated results are similar, especially in stage 5 with the ADALINE-based control scheme. Calculated copper losses per phase P_{loss} with MTPA (stage 3) are significantly different from 1.21 to 1.88 *pu*. Those values of RCA (stages 4 and 5) dramatically vary from 1.11 to 4.45 *pu*. By using optimal currents, MTPA generates a lower calculated total copper loss P_{loss_total} (1.25 *pu*) compared to the proposed RCA (2.30 *pu*) but with higher torque ripples.

To conclude, the proposed ADALINE-based control scheme using RCA has much better post-fault torque quality than the pre-fault scheme using MTPA. However, RCA results in a higher maximum peak current and a higher total copper loss.

C. Experimental results

The speed of the experimental drive is limited to 350 rpm due to the limit of DC-bus voltage 200 V as described in Table III. If the speed is higher, the proposed control scheme could be more effective as previously presented in the numerical result section (Fig. 8a). In addition, experimental torques are derived from measured currents and estimated NS-EMFs.

Fig. 9 shows the torque performance in the 5 operating stages (as in the numerical result section) at 100 rpm and 350 rpm. The experimental torque ripples (ΔT_{exp}) are higher than the numerical ones (ΔT_{cal} and ΔT_{sim}). The main reason is that the experimental NS-EMFs contain extra harmonics such as 11th and 13th (see Fig. 7b), causing more torque ripples. However, in general, the experimental torques are in good accordance with the numerical torques.

In Fig. 9a, the pre-fault control scheme at 100 rpm well performs regardless of time-variant reference currents. Therefore, the effectiveness of the proposed control scheme is not clear at 100 rpm. When the rotating speed increases to 350 rpm in Fig. 9b, the pre-fault control scheme no longer properly functions with varying references, leading to an increase in torque pulsation. Specifically, in healthy mode, the experimental torque ripple is at about 12.3%. When phase *A* is opened without any reconfigurations, the torque ripple increases to about 55.7%. The torque ripple slightly declines to 36% when new reference currents by MTPA are imposed. Without changing the control scheme, RCA generates a torque ripple of 27.9%. Finally, with the proposed control scheme using RCA, the torque ripple significantly decreases to 18.5%.

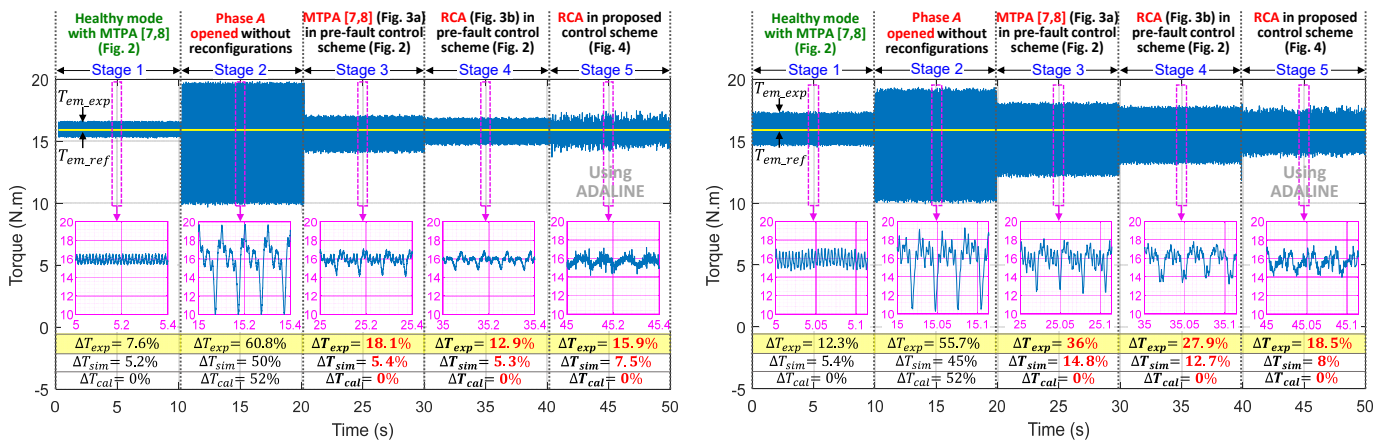

(a) (b)

Fig. 9. (Experimental results) Torque performance in five operating stages at 100 rpm (a), and at 350 rpm (b).

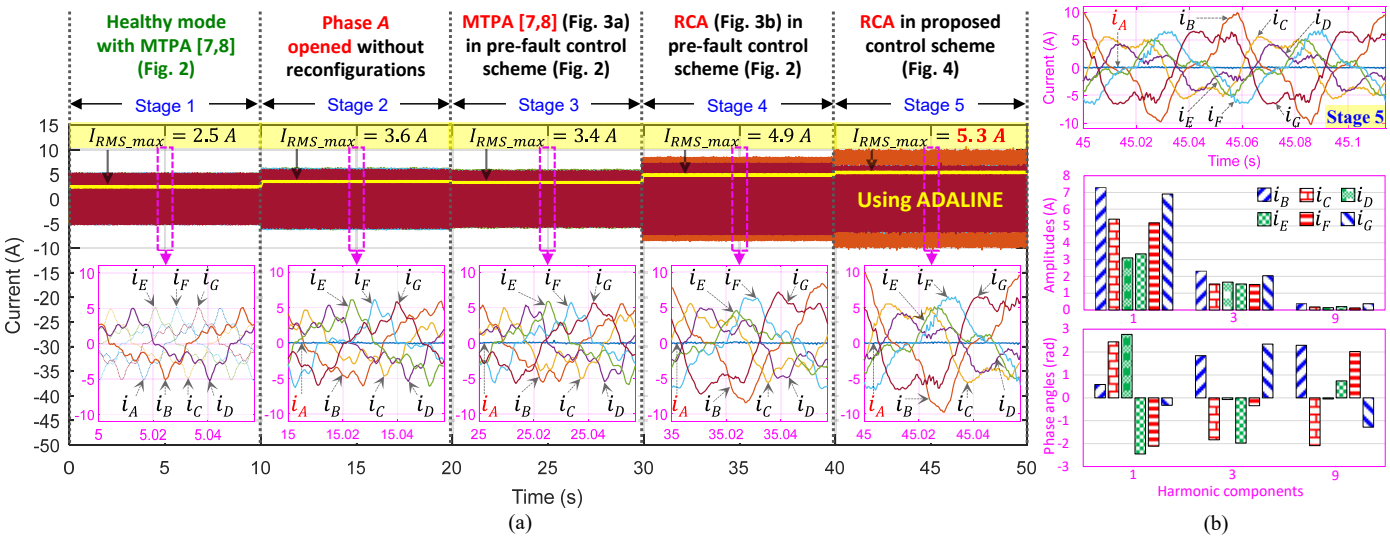

Fig. 10. (Experimental results) Measured phase currents in five operating stages at 350 rpm (a), zoomed measured phase currents in stage 5 with amplitudes and phases of their harmonic components (1st, 3rd, 9th) (b).

The experimental torque ripples of stages 3 to 5 are compared with the corresponding numerical results in Table IV. Notably, as the numerical results, MTPA generates higher experimental torque ripples than RCA in the pre-fault control scheme. In addition, the proposed control scheme results in better torque quality compared to the pre-fault control scheme. As previously discussed in section III.*B*, strategy RCA is a solution to deal with torque ripples in the first group strategies [2-6]. Indeed, under the same machine-drive conditions as in this study, study [5] with RFOC imposes constant currents (i_{d1}, i_{q1}, i_{d3}, i_{q3}) to generate most of the torque. Currents i_{d9} and i_{q9} are forcedly time-variant. With the 9th harmonic of NS-EMF at 32.3%, a torque ripple of 33% is generated at 191 rpm. Meanwhile, the proposed strategy RCA without or with the ADALINE-based control scheme has lower torque ripples of 27.9% and 18.5% at 350 rpm, respectively.

Like numerical results, the maximum peak and RMS currents created by RCA in stage 5 of Fig. 10a are highest (9.8 A and 5.3 A, respectively). Experimental copper losses of MTPA (stage 3) and RCA (stages 4 and 5) compared to healthy mode (stage 1) are summarized in Table V. It is noted that the experimental results are in good accordance with the numerical values. RCA leads to highest differences in experimental copper losses per phase (1.03 to 4.82 *pu* in stage 5). The total copper loss with MTPA (1.23 *pu*) is much less than that of RCA (2.10 *pu* in stage 4 and 2.32 *pu* in stage 5). Despite higher torque quality, strategy RCA owns a higher maximum peak current and a higher total copper loss than MTPA. This can be limitations of this proposed strategy.

The remaining healthy phase currents and their harmonic spectrum in the proposed ADALINE-based control scheme with RCA (stage 5) are presented in Fig. 10b. Measured phase currents are like their reference currents in Fig. 8b. Each measured phase current includes harmonic components with corresponding amplitudes and phase angles. In general, these measured phase currents mainly contain the first and third harmonics with different amplitudes and phase angles as previously described in (19)-(30). For example, among the remaining phases, amplitudes of the first and third harmonic components of currents of phases *B* and *G* are highest in Fig. 10b. Especially, tiny proportions of the 9th harmonic components are found in measured phase currents. These harmonics are created by the 9th harmonic components of the NS-EMFs.

In the pre-fault control scheme, current responses are unable to properly track their varying references with PI controllers at 350 rpm. For example, currents i_{q1}, creating most of the torque, cannot be sufficiently controlled in the pre-fault scheme with either MTPA (stage 3) or RCA (stage 4) as described in Fig. 11a. In contrast, the proposed ADALINE-based control scheme with RCA has significantly better tracking performance with time-constant references as plotted in Figs. 11b and 11c, leading to the lowest torque ripple in stage 5 of Fig. 9b. Indeed, the control performance of currents (i_{d11}, i_{q11}), generating most of the torque, and currents (i_{d91}, i_{q91}, i_{x1}) is of a high quality as presented in Fig. 11b. Notably, currents (i_{d11_est}, i_{q11_est}, i_{d91_est}, i_{q91_est}, i_{x1_est}) have no high-frequency components from measurements because these currents are obtained from the extracted currents (i_{B1_est}, i_{C1_est}, i_{D1_est}, i_{E1_est}, i_{F1_est}, i_{G1_est}) as described in RTCL of Fig. 4. Meanwhile, (i_{d33_est}, i_{q33_est}, i_{d93_est}, i_{q93_est}, i_{x3_est}) in Fig. 11c have high-frequency components. Indeed, (i_{C3_est}, i_{D3_est}, i_{E3_est}, i_{F3_est}, i_{G3_est}) are derived from differences between measured phase currents and extracted currents (i_{C1_est}, i_{D1_est}, i_{E1_est}, i_{F1_est}, i_{G1_est}) as described in RTCL block of Fig. 4.

To implement the proposed control scheme, main harmonics of i_{B_mea} are extracted with the proposed ADALINE as described in Fig. 12a. In the 5-stage operation, the learning process starts in stage 4 to prepare for stage 5. Then, weights can be automatically updated in response to variations of speed or torque. Four weights with learning rate η=0.01 converge to four coefficients of current harmonic components in (32) within 0.212 s (see Zoom 1). Then, current harmonic components (i_{B1_est}, i_{B3_est}) are extracted from i_{B_est} (i_{B_mea}) as

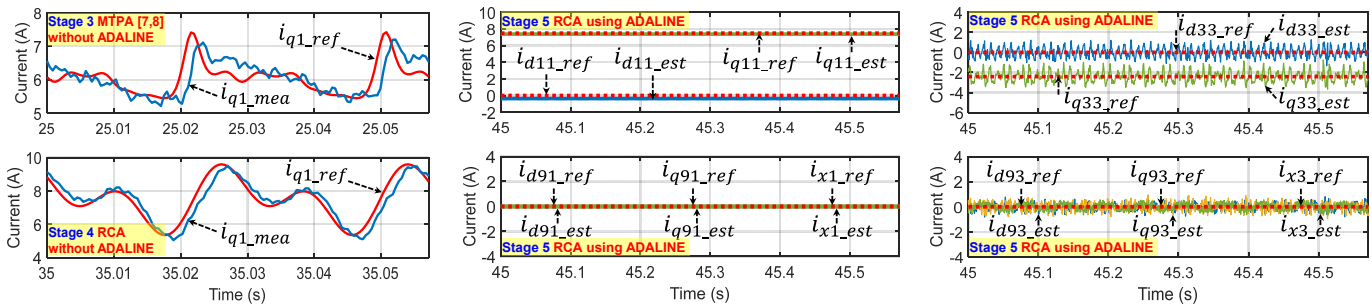

Fig. 11. (Experimental results) Current control performance at 350 rpm: current i_{q1} in the pre-fault control scheme with MTPA [7, 8] (stage 3) and the proposed RCA (stage 4) (a), currents (i_{d11}, i_{q11}, i_{d91}, i_{q91}, i_{x1}) (b) and (i_{d33}, i_{q33}, i_{d93}, i_{q93}, i_{x3}) (c) in the proposed ADALINE-based control scheme with RCA (stage 5).

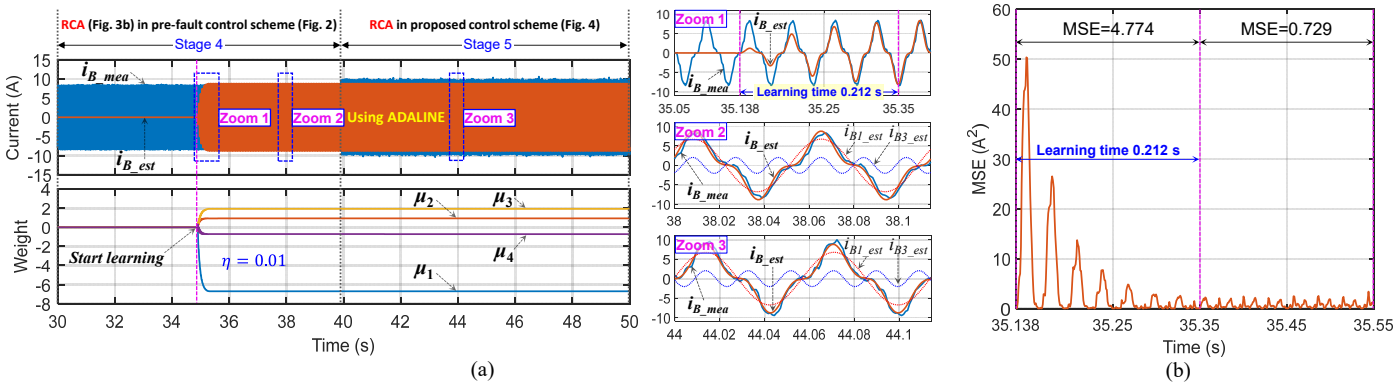

Fig. 12. (Experimental results) Learning the measured current of phase B ($i_{B\_est} \approx i_{B\_mea}$) in stages 4 and 5 at 350 rpm, ADALINE weight convergence with learning rate η=0.01, extracted current harmonic components i_{B1_est} and i_{B3_est} (a), MSE of the ADALINE calculated from Zoom 1 (b).

described in Zooms 2 and 3 of Fig. 12a. Suitable learning rates need to be determined according to the sampling time of calculations, desired current characteristics such as amplitudes. In this study, these values are chosen between 0.005 and 0.05 in experiments. If the learning rate is higher, the system instability may appear when the reference torque varies. Based on Zoom 1, MSE is calculated to evaluate the accuracy of the ADALINE as described in Fig. 12b. MSE reduces from 4.774 in the learning period to 0.729 after the learning period.

The dynamic performance of the proposed ADALINE-based control scheme with RCA (stage 5) under variations of the rotating speed and reference torque is shown in Fig. 13. Specifically, in Fig. 13a, the speed controlled by the Parvex load machine varies between 250 rpm and 350 rpm. For a reference torque of 15 N.m, the 7-phase PMSM is smoothly controlled with torque ripples of 21% and 22%. As previously discussed in subsection V.*B*, the rotating speed variations theoretically do not lead to variations in amplitudes and phase shift angles of current harmonic components. Only ADALINE inputs using sin(θ), cos(θ), sin(3θ), and cos(3θ) change. Therefore, four weights are almost unchanged in response to rotating speed variations. This characteristic can be experimentally confirmed by currents (i_{B_mea}, i_{B_est}) and weights (see Zooms 1, 2, and 3). An increase in the learning rate η (0.005 to 0.05) results in a shorter learning time (0.14 s to 0.028 s).

In Fig. 13b, the rotating speed is controlled at 300 rpm and the reference torque varies between 0 and 10 N.m. The torque ripple is 23% when T_{em_ref} is 10 N.m. Reference torque variations lead to changes in phase current amplitudes. In this case, four weights dramatically change in response to reference torque variations. This statement can be experimentally validated by currents (i_{B_mea}, i_{B_est}) and weights (see Zooms 1, 2, and 3). An increase in the learning rate η (0.005 to 0.05) results in a shorter learning time (0.78 s to 0.07 s), leading to shorter transient periods of the torque control.

To sum up, from the numerical and experimental results, the proposed ADALINE-based control scheme using RCA has much better post-fault torque quality compared to the pre-fault control scheme using MTPA. It is thanks to robustness of RCA and the use of constant reference d-q currents for control. However, a higher maximum peak current as well as a higher total copper loss are two limitations of the proposed strategy RCA.

VII. Conclusion

This paper has proposed a fault-tolerant strategy and a control scheme to obtain high-quality torque in single-phase open circuit faults. The proposed strategy RCA applying the reduced-order transformation approach can obtain a constant torque under the effect of multi-harmonics in NS-EMFs. To keep, in faulty as in healthy mode, the standard PI controllers with constant reference currents, a simple AI algorithm is used. It is based on an ADALINE which has the particularity to use the knowledge of NS-EMF harmonic ranks and the rotor position. Torque pulsations are then automatically reduced

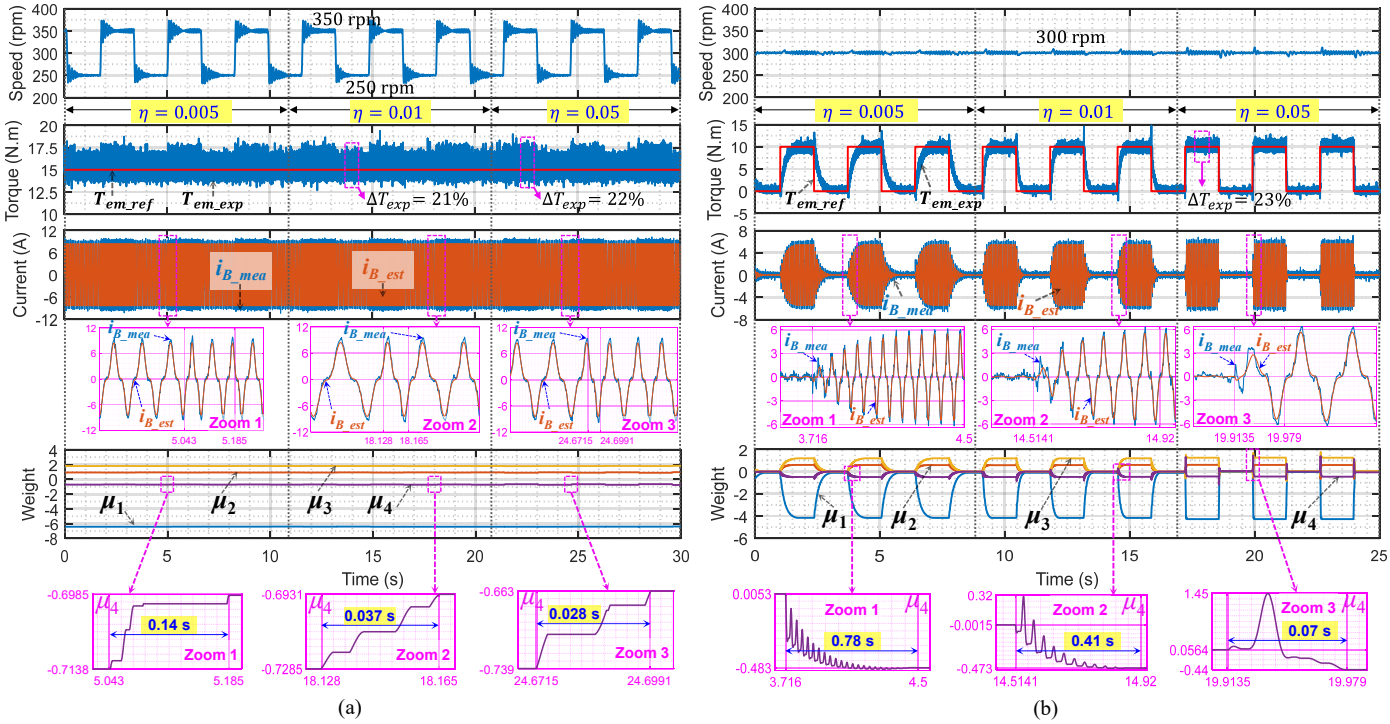

Fig. 13. (Experimental results) Electromagnetic torque, currents i_{B_mea} and i_{B_est} in learning process, ADALINE weights: under variations of the rotating speed (a), and under variations of the reference torque (b), when the proposed ADALINE-based control scheme with RCA is used for post-fault operation.

without the need of sensitive precise modeling. To experimentally evaluate the proposed control scheme, a non-sinusoidal (THD=38%) seven-phase machine has been chosen but this control scheme can be applied to other non-sinusoidal machines with different numbers of phases. When more phases are opened, the proposed control scheme can be adapted when new reduced-order transformation matrices are found. This can be a future work of this research topic. Therefore, faulty mode can be accepted as an operating option with high torque quality for non-sinusoidal industrial drives using PI controllers, supplied by non-sinusoidal currents.

References

[1] X. Kestelyn and E. Semail, "Vectorial Modeling and Control of Multiphase Machines with Non-salient Poles Supplied by an Inverter," in *Control of Non-conventional Synchronous Motors*, L. Jean-Paul, Ed.: Wiley, 2012, pp. 161-206.

[2] F. Jen-Ren and T. A. Lipo, "Disturbance-free operation of a multiphase current-regulated motor drive with an opened phase," *IEEE Transactions on Industry Applications,* vol. 30, no. 5, pp. 1267-1274, 1994.

[3] H. A. Toliyat, "Analysis and simulation of five-phase variable-speed induction motor drives under asymmetrical connections," *IEEE Transactions on Power Electronics,* vol. 13, no. 4, pp. 748-756, 1998.

[4] F. Locment, E. Semail, and X. Kestelyn, "Vectorial Approach-Based Control of a Seven-Phase Axial Flux Machine Designed for Fault Operation," *IEEE Transactions on Industrial Electronics,* vol. 55, no. 10, pp. 3682-3691, 2008.

[5] D. T. Vu, N. K. Nguyen, E. Semail, and T. J. d. S. Moraes, "Control strategies for non-sinusoidal multiphase PMSM drives in faulty modes under constraints on copper losses and peak phase voltage," *IET Electric Power Applications*, vol. 13, no. 11, pp. 1743-1752, 2019.

[6] Y. Sui, P. Zheng, Z. Yin, M. Wang, and C. Wang, "Open-Circuit Fault-Tolerant Control of Five-Phase PM Machine Based on Reconfiguring Maximum Round Magnetomotive Force," *IEEE Transactions on Industrial Electronics,* vol. 66, no. 1, pp. 48-59, 2019.

[7] S. Dwari and L. Parsa, "An Optimal Control Technique for Multiphase PM Machines Under Open-Circuit Faults," *IEEE Transactions on Industrial Electronics,* vol. 55, no. 5, pp. 1988-1995, 2008.

[8] X. Kestelyn and E. Semail, "A Vectorial Approach for Generation of Optimal Current References for Multiphase Permanent-Magnet Synchronous Machines in Real Time," *IEEE Transactions on Industrial Electronics,* vol. 58, no. 11, pp. 5057-5065, 2011.

[9] S. Dwari and L. Parsa, "Fault-Tolerant Control of Five-Phase Permanent-Magnet Motors With Trapezoidal Back EMF," *IEEE Transactions on Industrial Electronics,* vol. 58, no. 2, pp. 476-485, 2011.

[10] D. Flieller, N. K. Nguyen, P. Wira, G. Sturtzer, D. O. Abdeslam, and J. Mercklé, "A Self-Learning Solution for Torque Ripple Reduction for Nonsinusoidal Permanent-Magnet Motor Drives Based on Artificial Neural Networks," *IEEE Transactions on Industrial Electronics,* vol. 61, no. 2, pp. 655-666, 2014.

[11] A. Cervone, O. Dordevic, and G. Brando, "General Approach for Modeling and Control of Multiphase PMSM Drives," *IEEE Transactions on Power Electronics,* vol. 36, no. 9, pp. 10490-10503, 2021.

[12] R. Hyung-Min, K. Ji-Woong, and S. Seung-Ki, "Synchronous-frame current control of multiphase synchronous motor under asymmetric fault condition due to open phases," *IEEE Transactions on Industry Applications,* vol. 42, no. 4, pp. 1062-1070, 2006.

[13] H. Guzman *et al.*, "Comparative Study of Predictive and Resonant Controllers in Fault-Tolerant Five-Phase Induction Motor Drives," *IEEE Transactions on Industrial Electronics,* vol. 63, no. 1, pp. 606-617, 2016.

[14] B. Tian, Q. T. An, J. D. Duan, D. Y. Sun, L. Sun, and D. Semenov, "Decoupled Modeling and Nonlinear Speed Control for Five-Phase PM Motor Under Single-Phase Open Fault," *IEEE Transactions on Power Electronics,* vol. 32, no. 7, pp. 5473-5486, 2017.

[15] H. Zhou, W. Zhao, G. Liu, R. Cheng, and Y. Xie, "Remedial Field-Oriented Control of Five-Phase Fault-Tolerant Permanent-Magnet Motor by Using Reduced-Order Transformation Matrices," *IEEE Transactions on Industrial Electronics,* vol. 64, no. 1, pp. 169-178, 2017.

[16] L. Cheng, Y. Sui, P. Zheng, P. Wang, and F. Wu, "Implementation of Postfault Decoupling Vector Control and Mitigation of Current Ripple for Five-Phase Fault-Tolerant PM Machine Under Single-Phase Open-Circuit Fault," *IEEE Transactions on Power Electronics,* vol. 33, no. 10, pp. 8623-8636, 2018.

[17] B. Tian, G. Mirzaeva, Q. An, L. Sun, and D. Semenov, "Fault-Tolerant Control of a Five-Phase Permanent Magnet Synchronous Motor for Industry Applications," *IEEE Transactions on Industry Applications,* vol. 54, no. 4, pp. 3943-3952, 2018.

[18] H. Zhou, C. Zhou, W. Tao, J. Wang, and G. Liu, "Virtual-Stator-Flux-Based Direct Torque Control of Five-Phase Fault-Tolerant Permanent-Magnet Motor With Open-Circuit Fault," *IEEE Transactions on Power Electronics,* vol. 35, no. 5, pp. 5007-5017, 2020.

[19] T. Tao, W. Zhao, Y. Du, Y. Cheng, and J. Zhu, "Simplified Fault-Tolerant Model Predictive Control for a Five-Phase Permanent-Magnet Motor With Reduced Computation Burden," *IEEE Transactions on Power Electronics,* vol. 35, no. 4, pp. 3850-3858, 2020.

[20] M. Priestley, M. Farshadnia, and J. E. Fletcher, "FOC Transformation for Single Open-Phase Faults in the Five-Phase Open-End Winding Topology," *IEEE Transactions on Industrial Electronics,* vol. 67, no. 2, pp. 842-851, 2020.

[21] D. T. Vu, N. K. Nguyen, and E. Semail, "An Overview of Methods using Reduced-Ordered Transformation Matrices for Fault-Tolerant Control of 5-phase Machines with an Open Phase," in *2019 IEEE International Conference on Industrial Technology (ICIT)*, Melbourne, Australia, 2019, pp. 1557-1562.

[22] G. Liu, Z. Lin, W. Zhao, Q. Chen, and G. Xu, "Third Harmonic Current Injection in Fault-Tolerant Five-Phase Permanent-Magnet Motor Drive," *IEEE Transactions on Power Electronics,* vol. 33, no. 8, pp. 6970 - 6979, 2018.

[23] C. Xiong, H. Xu, T. Guan, and P. Zhou, "Fault-tolerant FOC for five-phase SPMSM with non-sinusoidal back EMF," *IET Electric Power Applications*, vol. 13, no. 11, pp. 1734-1742, 2019.

[24] C. Xiong, T. Guan, P. Zhou, and H. Xu, "A Fault-Tolerant FOC Strategy for Five-Phase SPMSM With Minimum Torque Ripples in the Full Torque Operation Range Under Double-Phase Open-Circuit Fault," *IEEE Transactions on Industrial Electronics,* vol. 67, no. 11, pp. 9059-9072, 2020.

[25] M. Bermudez, I. Gonzalez-Prieto, F. Barrero, H. Guzman, M. J. Duran, and X. Kestelyn, "Open-Phase Fault-Tolerant Direct Torque Control Technique for Five-Phase Induction Motor Drives," *IEEE Transactions on Industrial Electronics,* vol. 64, no. 2, pp. 902-911, 2017.

[26] W. Kong, M. Kang, D. Li, R. Qu, D. Jiang, and C. Gan, "Investigation of Spatial Harmonic Magnetic Field Coupling Effect on Torque Ripple for Multiphase Induction Motor Under Open Fault Condition," *IEEE Transactions on Power Electronics,* vol. 33, no. 7, pp. 6060-6071, 2018.

[27] F. Lin, Y. Hung, and M. Tsai, "Fault-Tolerant Control for Six-Phase PMSM Drive System via Intelligent Complementary Sliding-Mode Control Using TSKFNN-AMF," *IEEE Transactions on Industrial Electronics,* vol. 60, no. 12, pp. 5747-5762, 2013.

[28] N. K. Nguyen, D. Flieller, P. Wira, and D. O. Abdeslam, "Neural networks for phase and symmetrical components estimation in power systems," in *2009 35th Annual Conference of IEEE Industrial Electronics*, Porto, Portugal, 2009, pp. 3252-3257.

[29] H. X. Nguyen, T. N. Tran, J. W. Park, and J. W. Jeon, "An Adaptive Linear-Neuron-Based Third-Order PLL to Improve the Accuracy of Absolute Magnetic Encoders," *IEEE Transactions on Industrial Electronics,* vol. 66, no. 6, pp. 4639-4649, 2019.

[30] L. Wang, Z. Q. Zhu, H. Bin, and L. M. Gong, "Current Harmonics Suppression Strategy for PMSM with Non-Sinusoidal Back-EMF Based on Adaptive Linear Neuron Method," *IEEE Transactions on Industrial Electronics,* vol. 67, no. 11, pp. 9164-9173, 2020.

[31] E. Semail, X. Kestelyn, and A. Bouscayrol, "Right harmonic spectrum for the back-electromotive force of an n-phase synchronous motor," in *the 39th IEEE Industry Applications Conference*, Seattle, WA, USA, 10/2004, vol. 1, pp. 71-78.